Role of Mixed Layer Dynamics in Tropical North Atlantic Interannual Sea Surface Temperature Variability

ALLYSON RUGG

University of Colorado Boulder, Boulder, Colorado

GREGORY R. FOLTZ

NOAA/Atlantic Oceanographic and Meteorological Laboratory, Miami, Florida

RENELLYS C. PEREZ

Cooperative Institute for Marine and Atmospheric Studies, University of Miami, and NOAA/Atlantic Oceanographic and Meteorological Laboratory, Miami, Florida

(Manuscript received 8 December 2015, in final form 28 July 2016)

ABSTRACT

This study examines the causes of observed sea surface temperature (SST) anomalies in the tropical North Atlantic between 1982 and 2015. The emphasis is on the boreal winter and spring seasons, when tropical Atlantic SSTs project strongly onto the Atlantic meridional mode (AMM). Results from a composite analysis of satellite and reanalysis data show important forcing of SST anomalies by wind-driven changes in mixed layer depth and shortwave radiation between 5° and 10°N, in addition to the well-known positive wind–evaporation–SST and shortwave radiation–SST feedbacks between 5° and 20°N. Anomalous surface winds also drive pronounced thermocline depth anomalies of opposite signs in the eastern equatorial Atlantic and intertropical convergence zone (ITCZ; 2°–8°N). A major new finding is that there is strong event-to-event variability in the impact of thermocline depth on SST in the ITCZ region, in contrast to the more consistent relationship in the eastern equatorial Atlantic. Much stronger anomalies of meridional wind stress, thermocline depth, and vertical turbulent cooling are found in the ITCZ region during a negative AMM event in 2009 compared to a negative event in 2015 and a positive event in 2010, despite SST anomalies of similar magnitude in the early stages of each event. The larger anomalies in 2009 led to a much stronger and longer-lived event. Possible causes of the inconsistent relationship between thermocline depth and SST in the ITCZ region are discussed, including the preconditioning role of the winter cross-equatorial SST gradient.

1. Introduction

Sea surface temperatures (SSTs) in the tropical North Atlantic (TNA) affect the meridional movement of the intertropical convergence zone (ITCZ) and its band of heavy rainfall and cloud cover. Changes in the ITCZ's position, and the associated changes in atmospheric circulation, in turn influence rainfall in northeastern Brazil (Nobre and Shukla 1996) and the Amazon basin (Yoon and Zeng 2010). SSTs in the TNA also affect Atlantic tropical cyclone activity (Wang et al. 2006; Kossin and Vimont 2007), Pacific ENSO events (Ham et al. 2013), and the development of the boreal summer Atlantic Niño mode (Foltz and McPhaden 2010; Richter et al. 2013).

Significant progress has been made in understanding the coupled ocean–atmosphere processes that drive seasonal to decadal variations of TNA SST, with previous studies attributing much of the observed variability to changes in the surface heat flux and resultant thermodynamic air–sea coupling (Carton et al. 1996; Chang et al. 1997; Xie 1999; Chang et al. 2000; Czaja et al. 2002; Vimont 2010; Mahajan et al. 2010; Evan et al. 2011). Positive wind–evaporation–SST (WES) feedback tends to amplify SST and wind anomalies in the TNA and generate southwestward propagation of the coupled anomalies (Chang et al. 2000, 2001; Vimont 2010; Mahajan et al. 2010), although model experiments show

Corresponding author address: Gregory R. Foltz, NOAA/AOML, 4301 Rickenbacker Cswy., Miami, FL 33149.
E-mail: gregory.foltz@noaa.gov

DOI: 10.1175/JCLI-D-15-0867.1

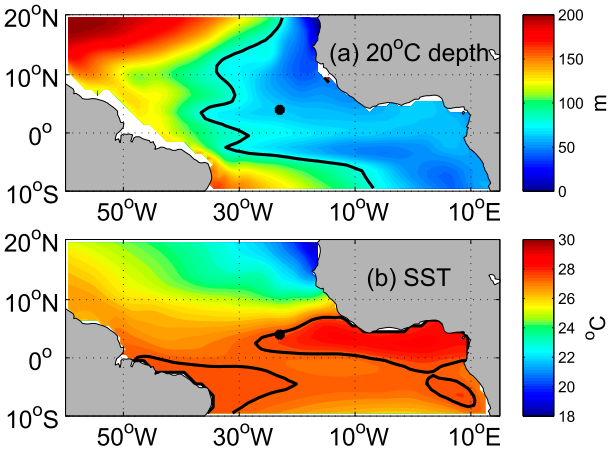

FIG. 1. March–May mean (1982–2014) (a) thermocline depth (defined as the depth of the 20°C isotherm, 80-m contour in black) and (b) SST, with 27.5°C contour in black. Black dots in (a) and (b) indicate location of the 4°N, 23°W PIRATA Northeast Extension mooring.

that significant SST and wind anomalies can exist without WES feedback (Mahajan et al. 2010). The external forcing of TNA SST and wind anomalies is thought to consist primarily of ENSO teleconnections (Enfield and Mayer 1997; Chang et al. 2000) and the NAO (Czaja et al. 2002) through changes in the strength of the trade winds. Horizontal temperature advection generally damps the thermodynamically driven SST anomalies (Chang et al. 2000; Xie 1999).

Surface heat fluxes alone cannot explain seasonal and interannual variations of SST between the equator and about 10°N, where the ITCZ is located (Carton et al. 1996; Yu et al. 2006; Foltz and McPhaden 2006; Hummels et al. 2014). In the western tropical Atlantic the thermocline is deep (Fig. 1a), tending to decouple the colder thermocline waters from the surface. In contrast, the shallow thermocline in the eastern tropical North Atlantic suggests that ocean mixed layer dynamics (i.e., changes in mixed layer depth, entrainment, and vertical mixing) may be important in this region. Indeed, recent studies indicate that mixed layer dynamics may contribute significantly to interannual variations of central and eastern TNA SST and associated movements of the ITCZ (Doi et al. 2010; Foltz et al. 2012). These studies focused on the Guinea Dome region (centered at about 12°N, 25°W) and used coupled model simulations (Doi et al. 2010) or investigated a single event using observations (Foltz et al. 2012). More comprehensive analysis is therefore needed to quantify the role of mixed layer dynamics in the evolution of TNA SST anomalies.

The ITCZ is most sensitive to SST anomalies during March–May, largely due to the high seasonal mean SST and weak meridional SST gradient during those months (Fig. 1b) (Chiang et al. 2002; Xie and Carton 2004; Hu and Huang 2006). Interannual SST variance is also highest in boreal spring in the TNA (Chiang et al. 2002; Czaja et al. 2002). While previous studies have emphasized the importance of air–sea coupling in the western tropical Atlantic warm pool region, conditions in the eastern TNA are also conducive to positive air–sea feedbacks during March–May. In the eastern Atlantic ITCZ region (2°–8°N, 15°–35°W), the average SST during March–May is 28.0°C (based on satellite SST data from 1998 to 2015), whereas in the western Atlantic ITCZ region (2°–8°N, 35°–50°W) SSTs average 27.4°C. The higher seasonal mean SST in the east means that atmospheric circulation may be more sensitive to SST anomalies in this region (Graham and Barnett 1987). Surface wind anomalies induced by SST anomalies in the eastern TNA during boreal spring can also have a significant influence on eastern equatorial Atlantic SSTs during the developing phase of the Atlantic Niño, which may feed back positively onto the meridional SST gradient and winds. Therefore, better knowledge of the drivers of March–May SST variability in the TNA, and specifically in the eastern portion of the basin, has the potential to improve our understanding of tropical Atlantic climate variability.

TNA SSTs during boreal spring project strongly onto the Atlantic meridional mode (AMM), typically defined either as the anomalous meridional SST gradient across 5°N (Servain 1991) or as the first joint EOF of SST and surface winds (Chiang and Vimont 2004), providing a convenient framework for analysis. Negative AMM events, with cold SST anomalies in the TNA and comparably warmer SSTs in the tropical South Atlantic, are associated with anomalously high surface wind speed (i.e., northeasterly wind anomalies) in the TNA and southward migration of the ITCZ (Figs. 2 and 3) (Nobre and Shukla 1996; Chiang and Vimont 2004). Conversely, positive AMM events are associated with negative wind speed anomalies (i.e., southwesterly wind anomalies) in the TNA and a northward displacement of the ITCZ. Here the evolution of the upper ocean during a typical AMM event is shown through composite analysis. Previous studies have found an important contribution from mixed layer dynamics in certain regions and during specific events (Doi et al. 2010; Foltz et al. 2012), but a broader observation-based analysis is lacking. Therefore, the main question that we seek to answer is whether mixed layer dynamics consistently and significantly affect SST during AMM events. In addition to a 33-yr satellite-era composite analysis, we investigate the role of mixed layer dynamics using direct measurements from 12 long-term moorings in the TNA and numerical

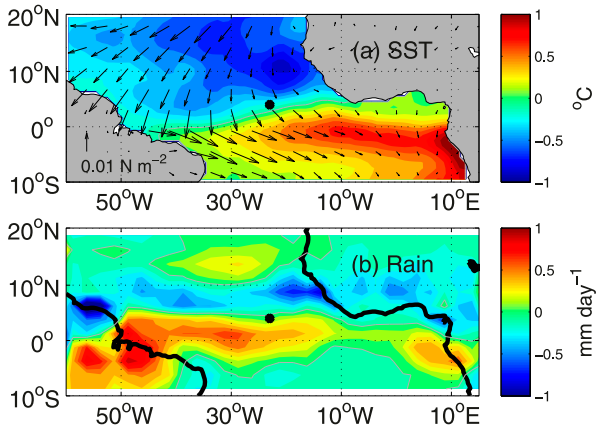

FIG. 2. Composite maps of AMM events during March–May for 1982–2014. Signs shown are for typical negative events. (a) SST anomalies (shaded) and wind stress anomalies (vectors). (b) GPCP rainfall anomalies (shaded).

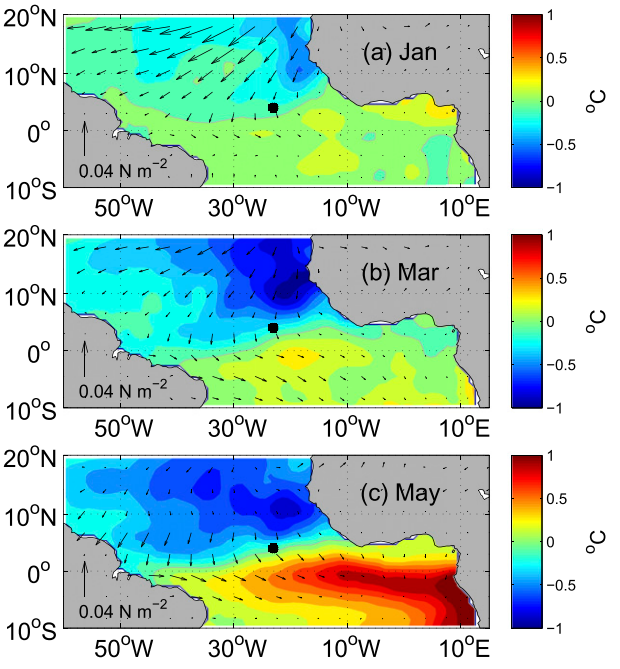

FIG. 3. As in Fig. 2a, but showing growth and decay using monthly means in (a) January, (b) March, and (c) May.

experiments with a mixed layer model. Particular attention is given to a strong negative AMM event in 2009, a weaker negative event in 2015, and a positive event in 2010.

2. Data

Satellite data, oceanic and atmospheric reanalyses, and in situ measurements from Prediction and Research Moored Array in the Tropical Atlantic (PIRATA; Bourlès et al. 2008) buoys are used to conduct analyses of upper-ocean conditions and causes of SST variability during AMM events between 1982 and 2015.

a. Satellite data and ocean reanalyses

We use the monthly combined satellite and in situ SST data on a 1° × 1° grid from 1982 to 2015 (Reynolds et al. 2002). The surface heat fluxes (latent, sensible, shortwave, and longwave) come from the daily TropFlux product (Praveen Kumar et al. 2012) on a 1° × 1° grid from 1982 to 2015. This dataset uses a combination of ERA-Interim winds and humidity (Dee et al. 2011), satellite SST and outgoing longwave radiation, and International Satellite Cloud Climatology Project–Flux Dataset (ISCCP-FD) surface shortwave and longwave radiation climatologies (Zhang et al. 2004). Wind velocity at a height of 10 m was obtained from the ERA-Interim reanalysis on a daily 0.75° × 0.75° grid from 1982 to 2015. These winds were also used to estimate the wind-driven vertical velocity [the methodology is described in section 3a(2)].

We obtained monthly 1° × 1° temperature and salinity for 1982–2014 from the European Centre for Medium-Range Weather Forecasts (ECMWF) Ocean Reanalysis System 4 (ORAS4; Balmaseda et al. 2013) to compute mixed layer depth (MLD) and thermocline depth (discussed in the following section 3). Our choice of ORAS4 is based on comparison of its monthly MLD and thermocline depth anomalies to those from NCEP's Global Ocean Data Assimilation System (GODAS; Behringer and Xue 2004) and the Simple Ocean Data Assimilation product (SODA; Carton and Giese 2008). Specifically, we found significantly better agreement between ORAS4 MLD and thermocline depth, and PIRATA MLD and thermocline depth, in the TNA. Here we define thermocline depth as the depth of the 20°C isotherm, and MLD is defined using a 0.07 kg m^{-3} density criterion [described further in section 3a(1)]. At the 4°N, 23°W; 4°N, 38°W; and 11.5°N, 23°W PIRATA mooring locations, where we anticipate MLD and thermocline depth anomalies may be important for SST (Doi et al. 2010, Foltz et al. 2012), correlations between monthly PIRATA thermocline depth and ORAS4 thermocline depth are 0.83–0.89, compared to 0.57–0.84 for GODAS and SODA. For MLD, the correlations are 0.35–0.61 for ORAS4 and 0.03–0.35 for GODAS and SODA. Comparisons are similar at the other off-equatorial PIRATA locations in the TNA (8°, 12°, 15°, and 20°N along 38°W; also 20.5°N, 23°W), while the three reanalysis products perform more comparably along the equator at 0°, 10°, 23°, and 35°W.

Monthly near-surface (15-m depth) currents were obtained from a synthesis of drifter velocities, altimetry, and wind products (Niiler et al. 2003; Lumpkin and

Garzoli 2011; Perez et al. 2012). This dataset is available at weekly intervals from 1993 to 2013 with 0.25° spatial resolution, and we averaged to monthly means. These near-surface currents are used directly to estimate the horizontal advection of temperature, and indirectly to estimate the vertical velocity at 15-m depth through use of the continuity equation. Although the data are available for only 21 years, compared to 33–34 years for the satellite and reanalysis products mentioned previously, the quality of the velocity synthesis product is significantly higher because it incorporates direct measurements of near-surface velocity. We therefore examine the possible role of horizontal advection through composite analysis for the shorter 21-yr period.

b. PIRATA moorings

We use daily measurements from the PIRATA Northeast Extension (PNE) Autonomous Temperature Line Acquisition System (ATLAS) mooring at 4°N, 23°W during 2006 through 2015 for a detailed analysis of conditions during three AMM events (2009, 2010, and 2015). The data consists of ocean temperature, salinity, and velocity as well as air temperature, relative humidity, wind velocity, rainfall, and shortwave radiation. Near-surface ocean velocity measurements are at a depth of 10 m. The mooring provides subsurface temperature data at 1, 10, and 13 m; every 20 m between 20 and 140 m; and 180, 300, and 500 m. Subsurface salinity data are available at 1, 10, 20, 40, 60, and 120 m. To fill some temporal gaps in the subsurface salinity data, we used daily-averaged data from a PNE Tropical Flex (T-Flex) mooring also located at 4°N, 23°W. This mooring was deployed in early 2015 as a test of the next generation of PIRATA mooring technology. The average location of the T-Flex mooring is approximately 8 km southeast of the ATLAS mooring.

Data gaps of a few weeks to months in surface salinity from the ATLAS mooring were common prior to 2009 and in 2012, 2014, and 2015. Salinity measurements at 10 m were less frequently missing, only commonly unavailable during 2006–08 and 2012. The data gaps in salinity and temperature were filled using a variety of methods. The T-Flex mooring had fewer gaps for most of 2015, so we used these time series to fill gaps in the ATLAS data whenever possible. Prior to 2015, when T-Flex data were not available, missing data above 20 m were filled in using the value at the next available depth after correcting it using the mean temperature offset between the two depths for the given calendar day. If an entire day of data was missing at all depths, we filled the gaps using the daily climatology created from the mooring data.

In addition, we use daily-averaged temperature, salinity, relative humidity, air temperature, winds, and surface radiation data from 11 other PIRATA moorings for comparison to the satellite- and reanalysis-based composite analysis. These moorings are located at 0°, 10°, 23°, and 35°W along the equator; 11.5° and 20.5°N along 23°W; and 4°, 8°, 12°, 15°, and 20°N along 38°W. The time series vary in length from 8 to 17 yr. Gaps in temperature and salinity were filled using the methodology described previously in this section. Shortwave radiation at each location north of 4°N was corrected for dust biases using the ''MERRA clear-sky'' technique of Foltz et al. (2013a).

3. Methods

This section details the methods used to analyze the upper-ocean conditions and causes of SST variability during observed AMM events. Two approaches are used: composite analysis using satellite and ocean reanalysis data, and analysis of time series from the PIRATA moorings.

a. Composite analysis

1) Temperature balance equation

The mixed layer temperature balance equation for the TNA can be written as

$$\frac{\partial T}{\partial t} = \frac{Q_0}{\rho c h} + r \quad \text{and} \tag{1}$$

$$r = -(\mathbf{v} \cdot \nabla T) + r_{\text{vert}} + \epsilon, \tag{2}$$

where $\partial T/\partial t$ is the observed temperature rate of change, Q_0 is the net surface heat flux that absorbed by the mixed layer, ρ is the density of the water, c is the specific heat capacity of the water, and h is the depth of the mixed layer. The term r is the oceanic contribution to the SST tendency, which is the sum of horizontal advection $-(\mathbf{v} \cdot \nabla T)$, vertical advection, entrainment, and diffusion r_{vert}, and uncertainties from the other terms that are calculated ϵ. Horizontal advection is calculated directly, while the vertical term is estimated qualitatively using the wind-driven vertical velocity and thermocline depth, and as the residual between $\partial T/\partial t$ and the sum of horizontal advection and the surface heat flux. In this case, errors are not separable from the vertical term.

We define the mixed layer depth as the depth at which density is 0.07 kg m^{-3} greater than at 5 m. Mixed layer depths computed using a 0.15 kg m^{-3} density threshold, and temperature-only 0.2° and 0.5°C thresholds, gave similar results. The turbulent and radiative heat fluxes from TropFlux were used to calculate the atmosphere's contribution to the temperature balance. The amount of

shortwave radiation absorbed by the mixed layer was calculated using the mixed layer depth and the monthly seasonal cycle of surface chlorophyll-a concentration provided by the Sea-Viewing Wide Field-of-View Sensor (SeaWiFS; Morel and Antoine 1994; Sweeney et al. 2005; Foltz et al. 2013b).

Horizontal advection was calculated using the monthly averaged drifter-altimetry synthesis data, combined with monthly horizontal SST gradients calculated from the satellite SST data using centered differences over distances of 0.25°. We do not account for horizontal eddy advection on time scales shorter than one month. Prior results from Foltz et al. (2012, 2013b) suggest that, when averaged to monthly means, eddy advection makes up less than 10% of the total advection during boreal winter and spring in the TNA. The total oceanic contribution to the SST tendency r is estimated as the difference between the SST tendency and the total heat flux terms in (1). This oceanic residual term is then compared to horizontal advection, thermocline depth (calculated as the depth of the 20°C isotherm), and estimates of wind-driven vertical velocity in order to determine the oceanic processes that are mostly likely to affect SST.

2) EKMAN PUMPING

Wind-driven vertical velocity was calculated from monthly ERA-Interim winds using a simple equatorially modified Ekman model applied by Perez et al. (2012) and Foltz et al. (2012). It can be expressed as

$$w_\tau = \frac{r_s \nabla \cdot \tau + f \nabla \times \tau}{\rho_0 (f^2 + r_s^2)} + \frac{\beta (f^2 - r_s^2)\tau_x - 2f\beta r_s \tau_y}{\rho_0 (f^2 + r_s^2)^2} \quad (3)$$

$$= w_{\text{div}} + w_{\text{curl}} + w_{\tau_x} + w_{\tau_y}, \quad (4)$$

where τ_x and τ_y are the zonal and meridional components of wind stress, ρ_0 is the seawater density, f is the Coriolis parameter, $\beta = \partial f/\partial y$, and $r_s = (1.5 \text{ days})^{-1}$ is the dissipation rate. From left to right, the terms in (4) represent the vertical velocity due to wind stress divergence, vertical component of the curl, zonal wind stress, and meridional wind stress. For $r_s = 0$, (3) simplifies to the classical Ekman pumping velocity $\nabla \times [\boldsymbol{\tau}/(\rho_0 f)]$.

For validation, we compared this to the divergence of the horizontal velocity from the drifter-altimeter product. The values are generally consistent, and the resulting AMM composites were similar between the two methods. Specifically, for validation we looked at the correlations between the area-averaged products from the two methods between 2° and 10°N and found that the January–February means had a correlation coefficient of 0.32 and the April–May means had a correlation coefficient of 0.72 (significant at the 99% level). The RMS difference in vertical velocity between the two methods is 0.019 and 0.029 m day^{-1} for the January–February and April–May means, respectively. These values are generally less than half of the maximum vertical velocity anomalies during a composite AMM event (shown and discussed in section 4).

3) COMPOSITING TECHNIQUE

The AMM index was obtained by first calculating SST averaged in the region 3°–20°N, 60°W–15°E minus SST in the region 10°S–3°N, 60°W–15°E and then removing the monthly mean seasonal cycle. The 3°N boundary was chosen based on the mean location of the ITCZ. This definition is similar to that used by Servain (1991) (SST averaged over 5°–28°N, 60°W–15°E minus 20°S–5°N, 60°W–15°E), although we place a slightly stronger emphasis on lower latitudes, which are likely to affect atmospheric circulation and rainfall most strongly. To determine the intensity of each AMM event, we averaged the AMM index during March–May for each year. The positive composite for each parameter was then calculated from the years in which the AMM index exceeded 0.3°C. The negative composite was calculated from the years in which the AMM index was less than −0.3°C. This results in six positive events and seven negative events during 1982–2014 (Fig. 4). The year 2015 also qualified as a negative event but is not included in the composite analysis because ORAS4 data are not available. Because of the high symmetry between the positive and negative composites, we show only the average composites (i.e., the sum of the seven negative events minus the sum of the six positive events, divided by 13). A negative sign was chosen for our composite because our one-dimensional mixed layer modeling and PNE mooring analyses focus primarily on two recent negative AMM events (although one positive event is also examined).

b. *PIRATA moorings*

The temperature balance analyses at the PIRATA mooring locations in many ways mirror the composite temperature balance analysis, with some important exceptions. First, daily averaged direct measurements from the moorings were used whenever possible. Second, correlation analysis is used for a basinwide assessment because some of the records are too short to generate composites. Finally, we examine the time series from 4°N, 23°W in added detail because of its unique location in a region of strong SST and thermocline depth variability during its decade-long deployment from 2006 to 2015.

Surface shortwave radiation is available directly from the moorings, and the amount absorbed in the mixed

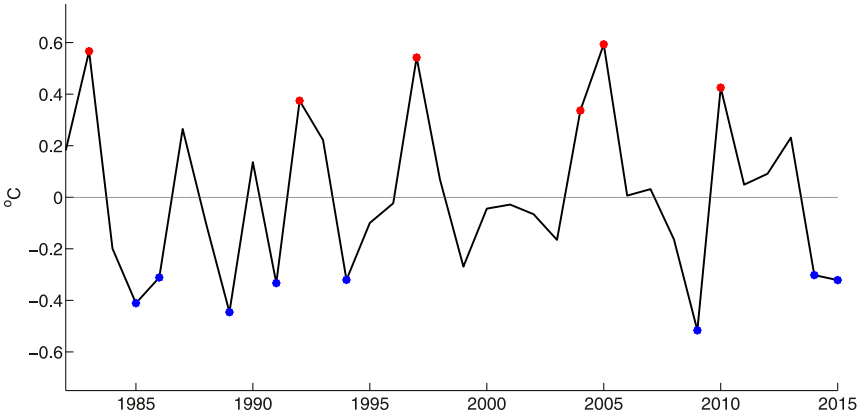

FIG. 4. AMM index from 1982 to 2015, computed as described in section 3a(3). Red and blue dots represent the years when the AMM index exceeded 0.3°C and was less than −0.3°C, respectively. These years (with the exception of the negative event in 2015) were used in the composite analysis.

layer is calculated using the methodology described in section 3a(1). MLD is also calculated with daily mooring temperature and salinity using the same methodology as in section 3a(1). We use daily downward longwave radiation from the ERA-Interim reanalysis and calculate the upward longwave component using the mooring SST. Latent and sensible heat fluxes were calculated from version 3 of the COARE algorithm (Fairall et al. 2003) using daily mooring SST, wind speed, air temperature, and relative humidity. To compute horizontal advection at 4°N, 23°W, we used the in situ velocity at 10-m depth together with satellite microwave SST gradients calculated over a distance of 0.25° using centered differences. We did not consider horizontal advection at the other mooring locations because direct measurements of horizontal velocity are often not available. ERA-Interim winds were used to estimate the wind stress curl at the 4°N, 23°W mooring site.

The 4°N, 23°W data were smoothed using a 20-day mean to eliminate short time scale variability. For terms such as advection, the low-pass filter was applied to the final product. For example, we smoothed $u\partial T/\partial x$, not u and $\partial T/\partial x$ separately. Monthly means of daily PIRATA data were used for the basinwide correlation analysis.

c. *One-dimensional mixed layer model*

We performed experiments with a one-dimensional mixed layer model (Price et al. 1986) in order to verify the role of vertical processes inferred from observations. Given surface heat, freshwater, and momentum fluxes, the model's mixed layer entrains successively deeper water until the bulk Richardson number exceeds 0.65. Vertical mixing is then performed beneath the mixed layer until the gradient Richardson number between each level is greater than 0.25. The model is initialized with temperature and salinity profiles from the 4°N, 23°W mooring and forced with wind stress, surface heat fluxes (except downward longwave radiation, which is from ERA-Interim), evaporation, and precipitation from the mooring. A time step of 15 min and vertical resolution of 1 m are used.

Three model experiments were performed with the goal of determining the portion of the observed SST anomalies at 4°N, 23°W that was driven by anomalous vertical turbulent mixing of upper-ocean temperature. The first experiment (FULL) was initialized with observed daily temperature and salinity from the mooring and forced with observed surface wind stress and fluxes of heat and moisture from the mooring. The second experiment (STRAT) is the same as FULL except climatological surface wind stress and heat/moisture fluxes were used to force the model. The third experiment (SALIN) is the same as STRAT except the model was initialized with climatological ocean temperature. The STRAT and SALIN experiments isolate the importance of initial density stratification and salinity stratification, respectively, in the evolution of SST anomalies.

Because changes in stratification are likely due in large part to changes in Ekman pumping and remote forcing from equatorial waves that our model does not explicitly include, we ran the model in 1-month segments, starting on 1 January and ending on 31 May, reinitializing on the first of every month. The experiments therefore consist of a set of five 1-month integrations. In this way, we are "relaxing" the model's subsurface temperature and salinity to observations at the start of each month. Because it takes Rossby waves several months to cross the basin at 4°N, this remote forcing is implicitly included in our simulations. The model does not explicitly resolve Ekman pumping (and associated vertical temperature advection) or submonthly variations in stratification

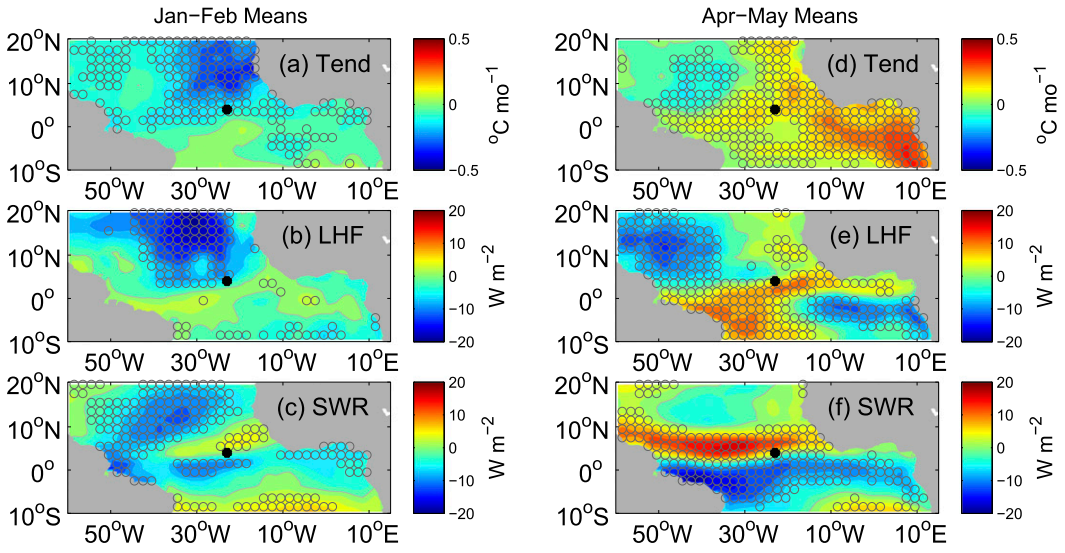

FIG. 5. Bimonthly composite anomalies for (a)–(c) January–February and (d)–(f) April–May: (a),(d) SST tendency, (b),(e) latent heat flux, and (c),(f) shortwave radiation. Here and in subsequent figures, values significant at the 90% confidence level (based on the Student's *t* test) are indicated with gray circles.

and their effects on SST. The model experiments therefore test the extent to which SST anomalies can be explained by the net surface heat and freshwater fluxes, and wind stress–induced mixing, acting on slowly evolving upper-ocean stratification.

The initial conditions for each month are the 10-day averaged temperature and salinity centered on the first day of each calendar month. Each model experiment was performed for 2009, 2010, and 2015 (a strong negative AMM event, strong positive event, and weaker and shorter-lived negative event, respectively), giving a total of 45 runs (three experiments for each of three years, and five months for each year).

4. Results

This section describes the results of the large-scale composite and PIRATA correlation analyses in the TNA, followed by the results of the time series analysis at the 4°N, 23°W mooring location and the one-dimensional modeling experiments at the same location.

a. Composite analysis

We first consider the heat exchange between the ocean and atmosphere, followed by ocean dynamics. Throughout this section we refer to the negative AMM composite, calculated as described in section 3a(3).

1) ATMOSPHERIC HEAT FLUXES

Consistent with previous studies, anomalies in the surface latent heat flux are the main precursor to boreal spring AMM events, especially north of 5°N. A strong anomalous cooling tendency in the TNA during January–February (Fig. 5a) is generated to a large extent by stronger than normal trade winds (Fig. 3a) and associated anomalous cooling from the latent heat flux (Fig. 5b). Shortwave radiation anomalies during January–February are confined mainly to the northwestern basin, the eastern ITCZ region and Gulf of Guinea, and between 5° and 10°S (Fig. 5c). The anomalies are consistent with positive low cloud–SST feedback in the northwestern and southern tropical Atlantic (Tanimoto and Xie 2002) and a southward shift of high cloudiness in the ITCZ.

As the SST anomalies develop, a negative feedback appears as colder waters lose less heat to evaporation than warmer waters (Figs. 5d,e). This effect is strong enough in April and May that the latent heat flux generates an anomalous warming tendency in the TNA, which acts to damp the SST anomalies (Fig. 5e). In April and May, shortwave radiation plays a more important role across the basin between 10°S and 10°N (Fig. 5f), while the negative shortwave radiation anomalies in the northwestern basin diminish. Colder than normal SSTs north of the equator and slightly warmer than normal SSTs on and south of the equator drive a southward displacement of the ITCZ (Fig. 2b). As a result, cloudiness is anomalously low between the equator and 10°N and high between the equator and 10°S, resulting in the observed pattern of shortwave radiation anomalies. The shortwave radiation fluxes strongly damp SST anomalies, especially between 3° and 8°N, the approximate mean latitude range of the ITCZ. Longwave radiation

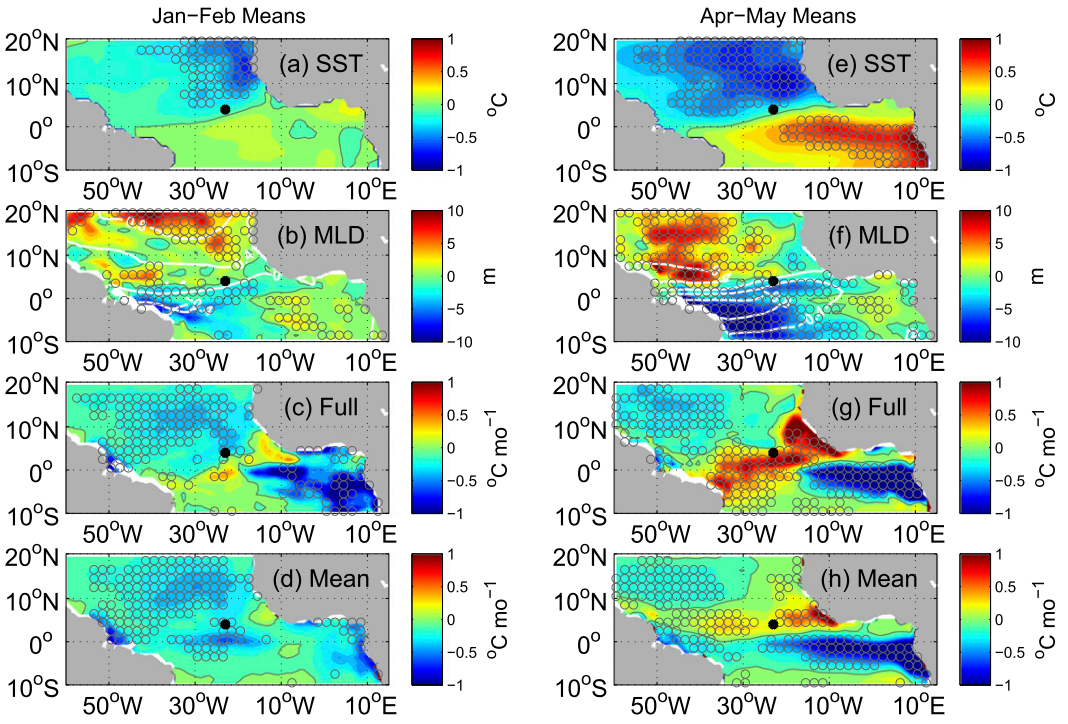

FIG. 6. Atmospheric and mixed layer depth anomaly composites for negative AMM events, showing (left) January–February averages and (right) April–May averages: (a),(e) SST; (b),(f) MLD, negative values indicate shallower mixed layer, and white contours show wind speed anomaly composites; (c),(g) combined shortwave and latent heating anomalies using the full observed MLD; and (d),(h) combined shortwave and latent heating anomalies using only the climatological MLD.

damps the SST anomalies with an amplitude much smaller than that of shortwave. For comparison, longwave radiation anomalies (not shown) are about a factor of 2 smaller in watts per meter squared, and a factor of 4 smaller in degrees Celsius per month, compared to latent and shortwave anomalies. Sensible heat fluxes were negligible compared to other heat fluxes.

Combined, the total atmospheric heat flux in the off-equatorial TNA strongly contributed to the initial development of the SST anomalies and later damped them in the eastern basin, tending to return SST to its mean state in April and May. In contrast, the net surface heat flux between 5°S and 5°N consists mainly of damping by shortwave radiation in April and May, and to a lesser extent in January–February. This is consistent with previous studies that show very weak correlations between the surface heat flux and SST tendency in this region and suggest that the SST tendency may be controlled more by ocean dynamics (Carton and Huang 1994; Carton et al. 1996; Foltz and McPhaden 2006; Foltz et al. 2012).

2) OCEAN DYNAMICS

Mixed layer depth is important in the development of the SST anomalies in some regions. We found anomalously thick mixed layers coinciding with cold anomalies, especially during January–February as the SST anomalies were developing (Figs. 6a,b). The thicker mixed layer is likely a direct result of the wind speed anomalies (white contours in Fig. 6b), with stronger winds inducing more vertical mixing and entrainment. Consistent with this interpretation, the largest MLD anomalies are found in the northern TNA, where the surface wind anomalies are largest. The positive MLD anomalies in the TNA had only a minor impact on SST during January–February (cf. Figs. 6c,d) because the mean mixed layer is thick (60–70 m; not shown) and MLD anomalies are generally less than 10 m (Fig. 6b). In contrast, thinner than normal mixed layers in the western basin between 10°S and 3°N (Fig. 6b), likely due to reductions in wind speed and eastward upper-ocean mass transport along the equator, have a significant impact on SST (cf. Figs. 6c,d). Smaller than normal MLDs in this region, combined with a mean mixed layer that is 40–45-m thick, allow the positive mean net surface heat flux to heat the mixed layer more efficiently and generate anomalous warming of 0°–0.3°C month^{-1} (Fig. 6c), in contrast to anomalous cooling if MLD anomalies are not taken into account (Fig. 6d). In the eastern equatorial Atlantic, anomalously large

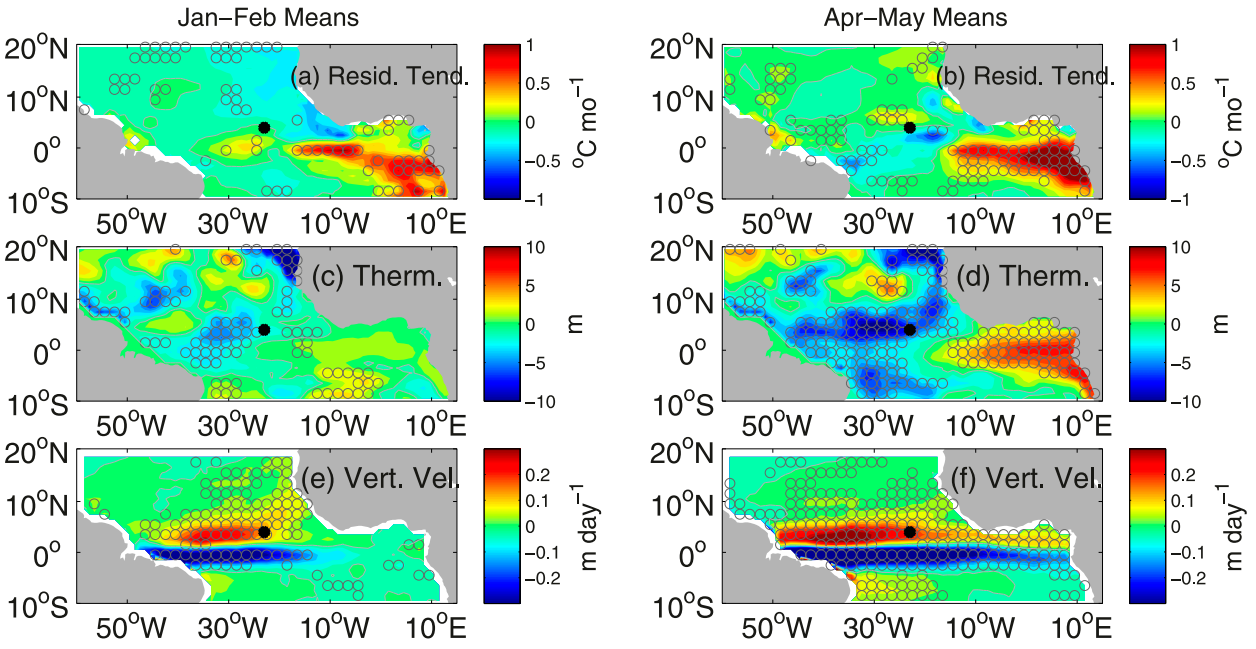

FIG. 7. Composites for negative AMM events: (a),(b) residual SST tendency anomalies (SST tendency minus the net surface heat flux); (c),(d) 20°C isotherm depth anomalies (negative values indicate shallower than normal isotherm); and (e),(f) Ekman vertical velocity anomalies, with positive defined as upward (i.e., positive anomalies indicate increased upwelling or decreased downwelling).

MLDs during January–February result in 0.5°–1°C more cooling compared to the case with climatological MLD (cf. Figs. 6c,d). The mean MLD is about 25 m in this region, explaining why surface heat flux–induced changes in SST are so sensitive to anomalies of MLD. The results are similar in April–May, except the region of strongest positive MLD anomalies in the TNA moves westward with the strongest SST and wind anomalies, and the negative MLD anomalies in the western basin intensify (Figs. 6e,f), likely due to stronger westerly wind anomalies along the equator. The contribution of anomalous MLDs to SST remains strong in the western basin between 10°S and 3°N (cf. Figs. 6g,h).

Taking anomalies of MLD into consideration, the surface heat flux drives most of the SST tendency anomalies between 2° and 20°N for a composite AMM. This can be seen in the maps of the residual (rate of change of SST minus the net surface heat flux) during a composite event (Figs. 7a,b), which show near-zero values during January–May. In contrast, there is an area of large positive residuals in a wedge stretching from the coast of Africa in the 10°S–2°N band and the equator at 15°W. This anomalous warming cannot be explained by the surface heat flux and is likely driven by anomalous deepening of the thermocline (Figs. 7c,d) and related anomalous warming of SST through a reduction in vertical turbulent cooling (Carton and Huang 1994). The anomalous deepening of the thermocline is more pronounced during April–May, when there is stronger anomalous Ekman downwelling (Figs. 7e,f) and positive Bjerknes feedback is likely stronger (Keenlyside and Latif 2007). We found that horizontal advection did not play an important role in the large-scale evolution of the residual anomalies, based on composites during the shorter 1993–2014 period (not shown), when reliable near-surface currents are available.

The thermocline is significantly shallower than normal between 10°S and 10°N in the central and western basin during April–May, consistent with upward anomalies of Ekman pumping between 2° and 10°N and generation of upwelling Rossby waves by equatorial wind anomalies and their reflections into equatorial Kelvin waves (Foltz and McPhaden 2010). Anomalously weak upwelling on the equator in the western basin (negative values in Figs. 7e,f), which would tend to deepen the thermocline anomalously, appears to be dominated by reflected upwelling Kelvin waves, which instead shoal the thermocline anomalously. There is evidence that local Ekman pumping contributes significantly between 2° and 10°N during January–May (Figs. 7e,f). Ekman pumping anomalies are about 0.05 m day^{-1} (1.5 m month^{-1}) averaged in the region during January–May, consistent with anomalous thermocline shoaling of approximately 5 m during the same period. However, processes that we did not explicitly address, such as coastal upwelling and Rossby wave propagation, seem to be important for

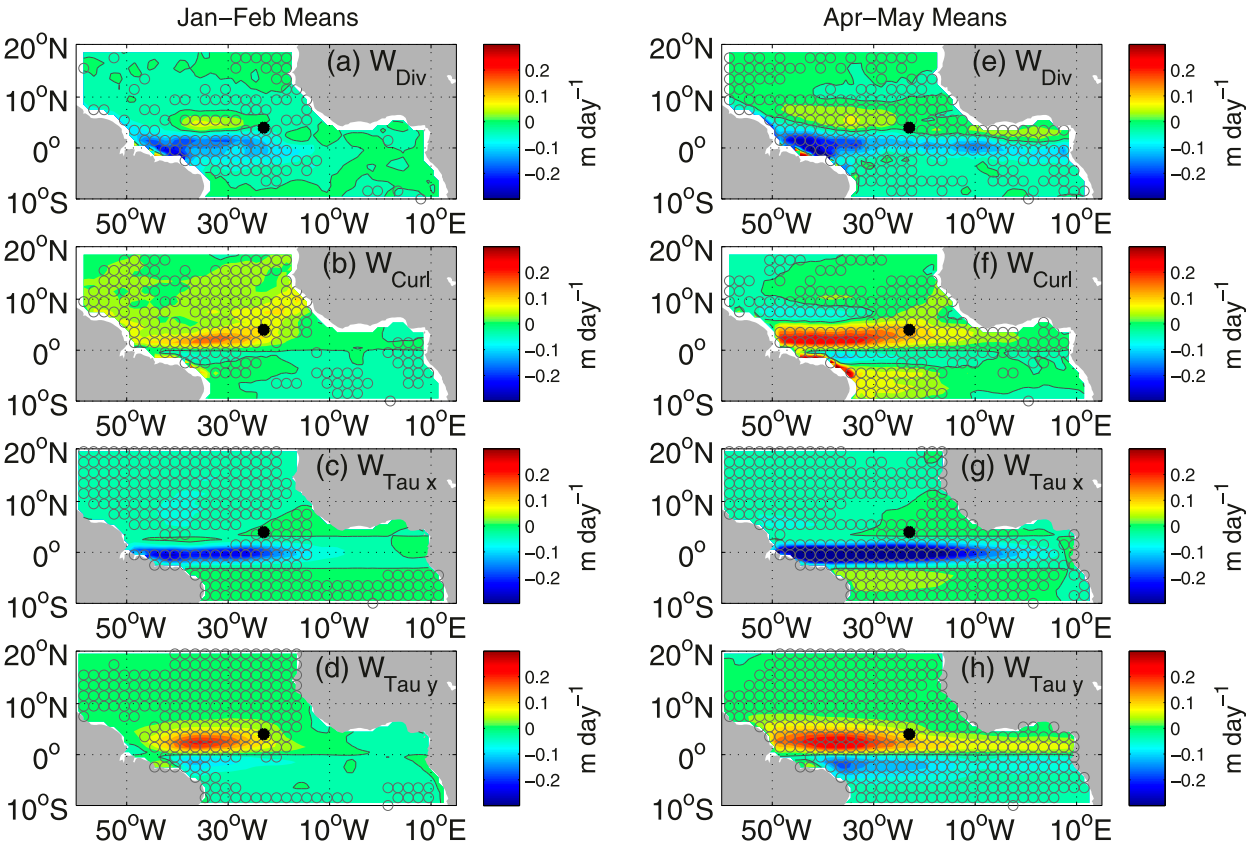

FIG. 8. Vertical velocity (positive upward) from the Ekman pumping [see (3)] during (a)–(d) January–February and (e)–(h) April–May of a composite negative AMM event. Terms are proportional to (a),(e) wind stress divergence, (b),(f) wind stress curl, (c),(g) zonal wind stress, and (d),(h) meridional wind stress.

explaining anomalous thermocline shoaling outside of this region (e.g., 15°–20°N, east of 30°W), given the weaker Ekman pumping velocities relative to the anomalous thermocline shoaling.

In a narrow band between 2° and 5°N, anomalous Ekman pumping is driven primarily by the w_{curl} and w_{τ_y} terms in (3) and (4), and both terms are strongest during April–May (Fig. 8). In contrast, near the equator (2°S–2°N) the w_{div} and w_{τ_x} terms dominate. These results are consistent with the pronounced meridional shifts of the ITCZ during AMM events, which drive anomalous meridional winds and wind stress curl in the ITCZ region, and anomalous SST in the eastern equatorial Atlantic that is linked to anomalous zonal winds along the equator (Figs. 2 and 3). In the Guinea Dome region (about 5°–12°N, 15°–30°W), wind stress curl is more important, consistent with Doi et al. (2010).

b. *PIRATA analysis*

Next, we use measurements from all PIRATA moorings in the TNA to validate the satellite- and reanalysis-based composite results. Monthly anomaly correlations between the AMM index and PIRATA latent heat flux, shortwave radiation, MLD, and thermocline depth (Z_{20}) generally support the conclusions drawn from the composite analysis (Fig. 9). During January–February of negative AMM events, latent heat flux tends to cool SST anomalously north of the equator and warm weakly on the equator (Fig. 9a). In contrast, during April–May there is anomalous warming from the latent heat flux in the eastern TNA and stronger warming along the equator (Fig. 9b), consistent with the composite analysis (Figs. 5c,d). Shortwave radiation is anomalously low on the equator and in the northwestern basin during January–February and anomalously high along 4°N and in the eastern TNA. In April and May the pattern is similar except negative shortwave anomalies are less widespread in the northwestern basin. These results also generally agree with those from the composite analysis (Figs. 5e,f), although the positive anomalies in the ITCZ are stronger for the composite. For the PIRATA analysis, MLD is generally thicker than normal in the TNA during January–May except in the extreme northeastern basin (Figs. 9e,f). The strongest positive

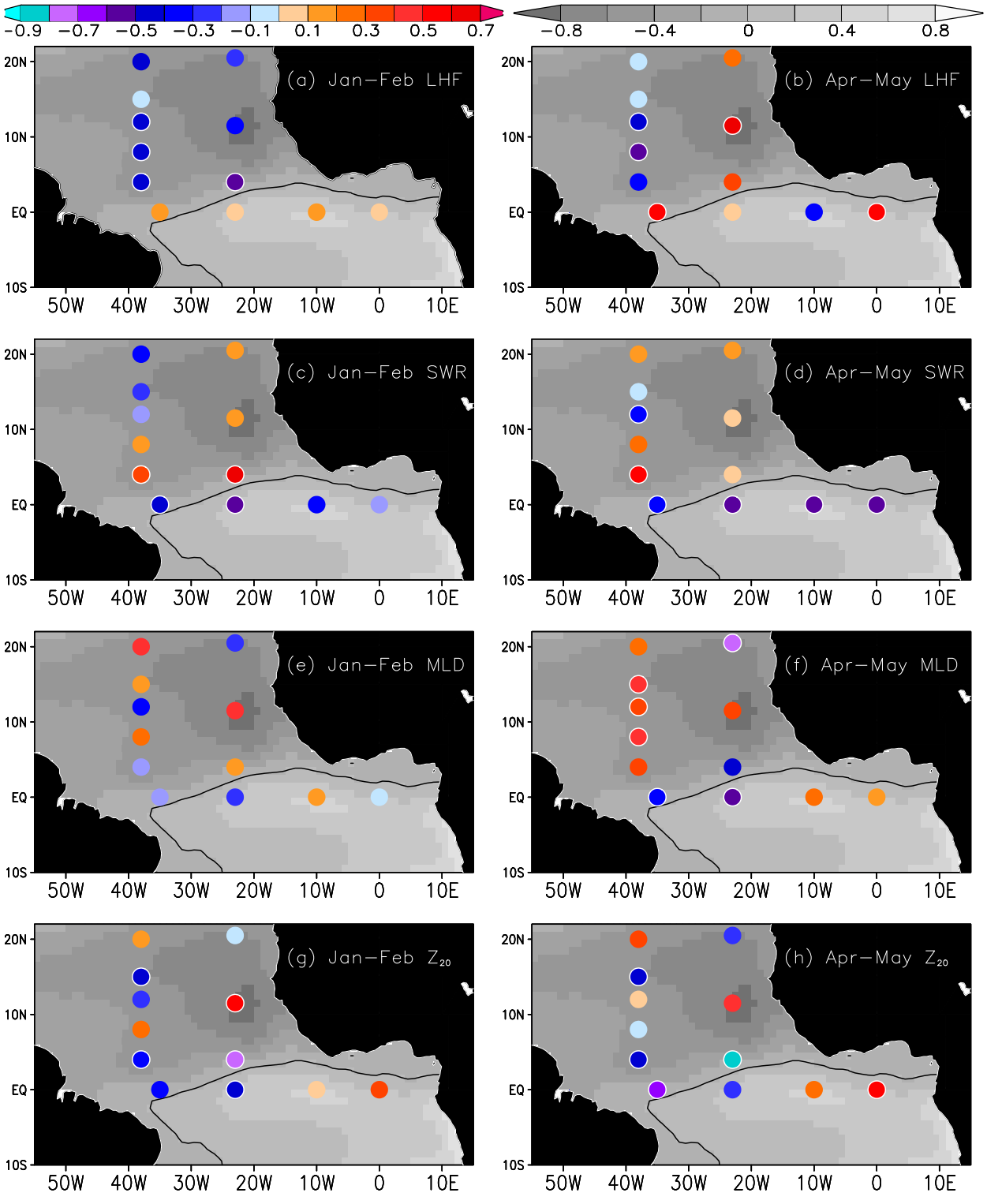

FIG. 9. Colored circles: monthly correlations between the negative AMM index (sign reversed for consistency with the negative AMM composites shown in Figs. 5–8) and (a),(b) LHF, (c),(d) SWR, (e),(f) MLD, and (g),(h) Z_{20} at each PIRATA mooring location during (left) January–February and (right) April–May. Correlations significant at the 90% level are indicated with white circles. In all panels, gray shading shows the March–May SST anomalies (°C) associated with the negative AMM composite, with black line indicating the zero contour.

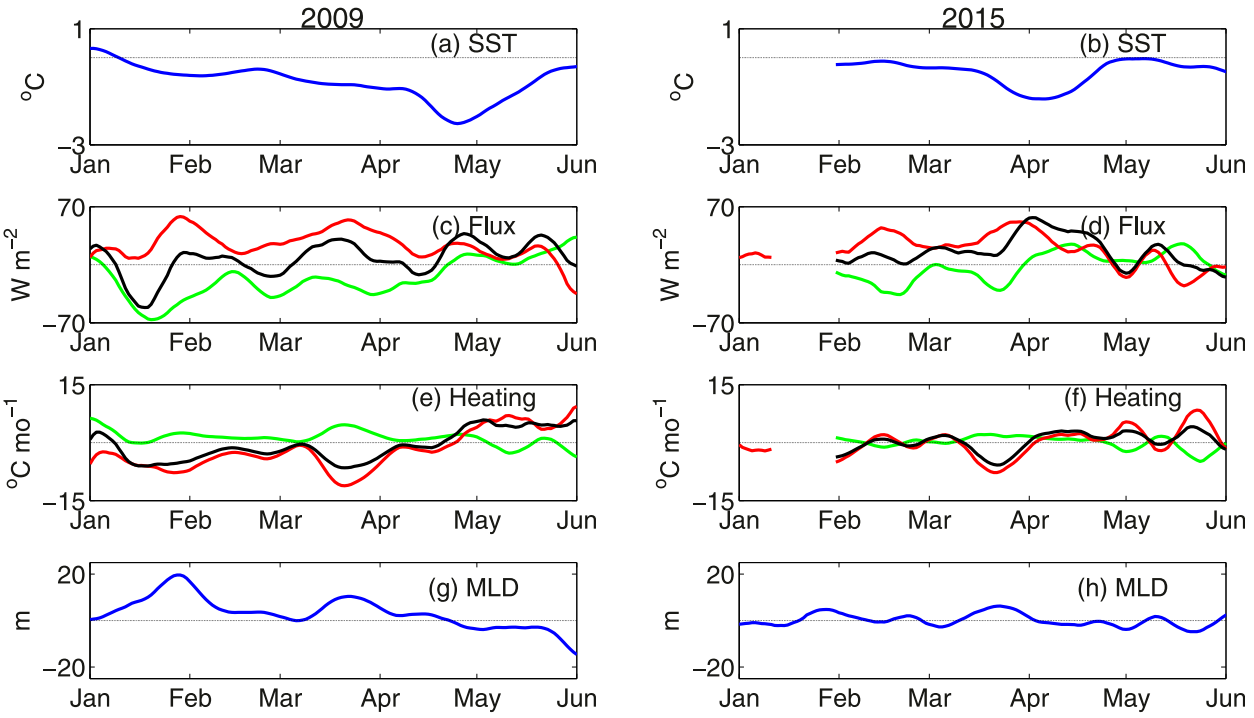

FIG. 10. Time series at 4°N, 23°W showing the importance of the mixed layer depth in determining the temperature change due to latent heat flux and shortwave flux during (left) 2009 and (right) 2015: (a),(b) SST anomalies and (c),(d) Latent (green) and shortwave (red) flux anomalies (W m^{-2}). Black curve represents the sum of latent and shortwave radiation contributions. (e),(f) As in (c),(d), but for the anomalous rate of SST change due to latent and shortwave flux anomalies. (g),(h) Mixed layer depth anomalies.

MLD anomalies in the PIRATA and the composite analyses are located in the western TNA during April–May (cf. Figs. 6b,f with Figs. 9e,f). The thermocline is anomalously shallow in the ITCZ region and in the western equatorial Atlantic during April–May in the PIRATA and composite analyses. Both analyses also show a shallower than normal thermocline in the northeastern basin and a mix of positive and negative values along 38°W (Figs. 7d and 9g,h).

Based on these comparisons, we have confidence in the main results from the composite analysis, which show the important damping effect of shortwave radiation within 10° of the equator, significant anomalous thickening of the mixed layer in the western TNA and thinning in the western equatorial Atlantic, and anomalous shoaling of the thermocline in the ITCZ region and deepening in the eastern equatorial Atlantic.

c. *PNE mooring at 4°N, 23°W*

Despite the significant negative anomalies in thermocline depth during April–May in the composite and correlation analysis, west of 15°W there is little evidence from the temperature balance residual (Fig. 7b) that the anomalously shallow thermocline affects SST. This contrasts with the results of Foltz et al. (2012), which show strong anomalous shoaling of the thermocline and resultant cooling from the vertical turbulent heat flux at the base of the mixed layer during January–April 2009. Their hypothesis was that Ekman pumping and associated shoaling of the thermocline bring anomalously cold water to the base of the mixed layer between the equator and 10°N. Vertical turbulent mixing then acts on the anomalous vertical temperature gradient, tending to cool the SST anomalously. This mechanism will be examined with mooring data at 4°N, 23°W in this section and tested with model experiments in section 4d. We focus on the negative AMM events of 2009 and 2015 (Fig. 4), when most of the terms in the SST budget are available from the mooring. While 2014 was also a strong negative AMM event, the PNE data for this time period are too sparse to use in our analysis.

1) EVOLUTION OF THE AMM EVENTS

In agreement with the PIRATA correlation analysis (Fig. 9), the time series from 2009 and 2015 both show anomalously high latent heat loss (tending to cool SST anomalously) early in the year as the cold SST anomalies develop (Figs. 10a,b and green lines in Figs. 10c,d). This is followed by anomalously low latent heat loss from late April to May in 2009 and early April through

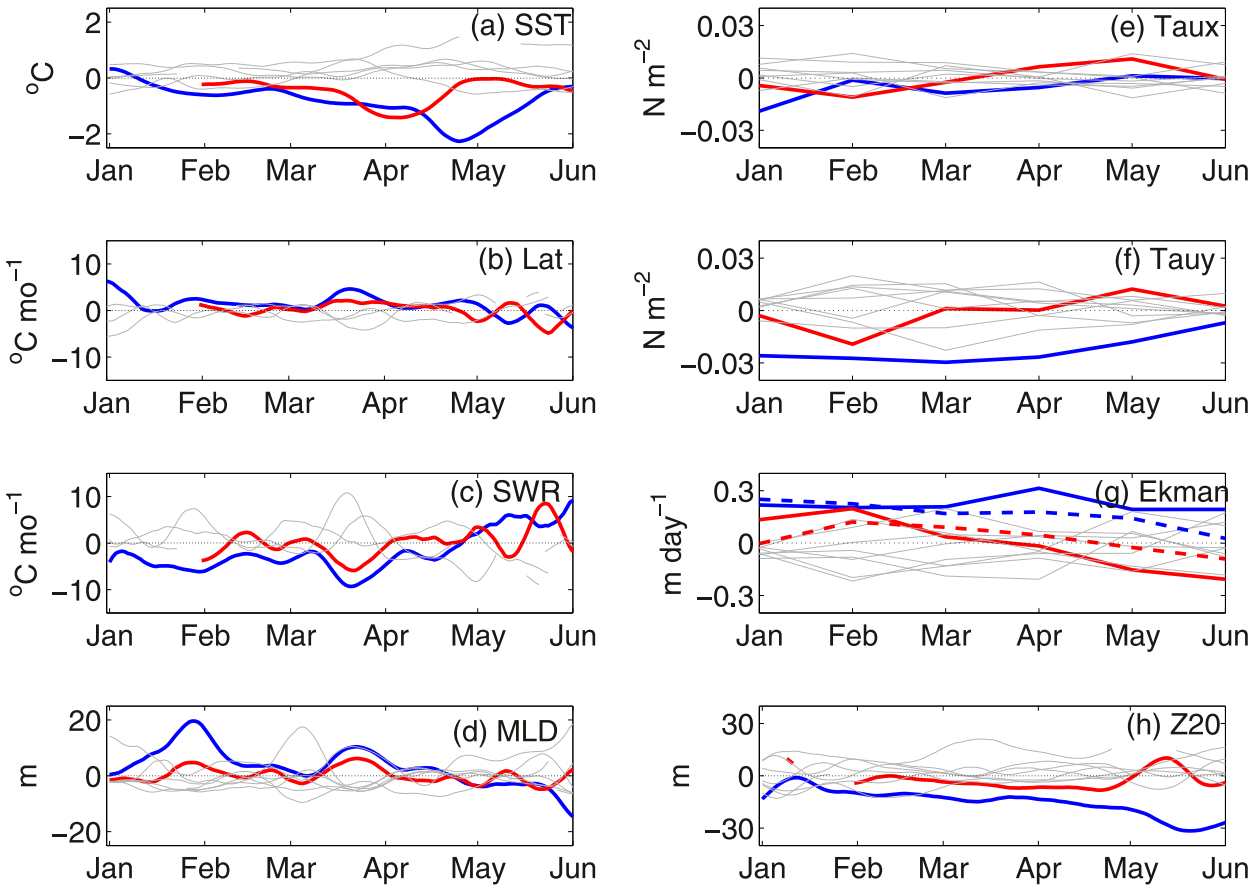

FIG. 11. Time series of 2009 (blue) and 2015 (red) anomalies at 4°N, 23°W, with all other years on record shown in gray: (a) SST; (b) SST change due to latent heat flux, negative values indicate anomalous cooling on mixed layer; (c) SST change due to shortwave radiation; (d) mixed layer depth; (e) zonal wind stress; (f) meridional wind stress; (g) Ekman vertical velocity, with dashed lines showing contributions from the w_{τ_y} term [see (3)]; and (h) 20°C isotherm depth.

May in 2015, as the SST anomalies reach their maximum intensities and begin to decay. Shortwave radiation anomalies are also consistent with the correlation analysis (red lines in Figs. 10c,d), showing a strong damping effect due to higher levels of incoming shortwave radiation in February–April of both years.

Mixed layer depth played an important role in the development of these events (Figs. 10e–h). The combined latent and shortwave heat flux anomaly is predominantly positive during February–April in both years (black lines in Figs. 10c,d), when the SST tendency anomaly is negative. However, the anomalous SST tendency induced by the total latent and shortwave fluxes (climatology plus anomaly) is negative on average during February–March of both years (black lines in Figs. 10e,f) because of the anomalously deep mixed layer (Figs. 10g,h). These results are generally consistent with the composite and correlation analyses (Figs. 6 and 9), which show a thicker than normal mixed layer at 4°N, 23°W during January–February and thinner than normal during April–May. We found that horizontal advection did not play a strong role during the buildup or decay of either event, although advection tended to cool SST anomalously by about 1°C in May 2015, after SST had returned to normal (this is discussed further in section 4d). In the next section, we examine the possible roles of vertical advection and mixing in the timing and intensity of the 2009 and 2015 events.

2) COMPARISON BETWEEN 2009 AND 2015

While 2009 and 2015 were negative AMM events, it is important to note that the 2015 cold event occurred earlier in the year, peaking in early April compared to late April in 2009 (Fig. 11a), and was less intense. We now discuss potential causes for these differences.

Although less cooling was observed in spring 2015 compared to 2009, heating from atmospheric heat transfer is very similar in both years (Figs. 11b,c). Mixed layer depth anomalies were also very similar with the exception of a much larger late January maximum in

2009 than in 2015 (Fig. 11d). Since atmospheric heating and mixed layer depth were so similar, and neither year had strong anomalies in horizontal advection (not shown), we turn to vertical processes to explain the difference between the 2009 and 2015 events.

During both events the meridional wind stress anomalies were generally stronger than the zonal components, especially during 2009 (Figs. 11e,f). The northerly wind stress anomalies during 2009 were the strongest on the 10-yr record during each month from January through June. These wind anomalies forced strong anomalous Ekman upwelling (Fig. 11g) and shoaling of the thermocline (Fig. 11h). In contrast, meridional wind stress anomalies were weaker in 2015, contributing to weaker anomalous upwelling that occurred over a shorter duration compared to 2009. As a result, thermocline depth anomalies in 2015 were much weaker than in 2009. These differences suggest that Ekman pumping and related thermocline shoaling may have played an important role in shaping the evolution of the 2009 and 2015 SST anomalies at 4°N, 23°W.

d. One-dimensional mixed layer model

The diagnostic analyses in the previous section suggest that anomalies of vertical processes (Ekman pumping and vertical mixing) may be important at 4°N, 23°W. Here we analyze output from the mixed layer model experiments to test this hypothesis. In addition to the 2009 and 2015 events discussed in the previous section, we consider the positive AMM event of 2010, for which surface fluxes, and subsurface temperature, and salinity for initialization are available from the mooring. We also performed the same experiments using surface forcing and initial conditions from the 4°N, 38°W mooring, which is in a region with significant thermocline depth anomalies during AMM events (Figs. 7 and 9). The results (not shown) show very small contributions from vertical processes in all years, consistent with a much deeper mean thermocline at this location (Fig. 1a) that limits the sensitivity of SST to thermocline depth anomalies. We therefore focus on the results from the experiments performed at 4°N, 23°W in this section.

1) COMPARISON TO OBSERVED SST

In general, the model with anomalous forcing (FULL experiment; blue squares in Fig. 12) reproduces the observed evolution of anomalous SST at 4°N, 23°W reasonably well during January–April in 2009, 2010, and 2015 (Fig. 12). There is about 2.5°C of anomalous cooling in the model from January to April 2009, consistent with observations (Fig. 12a). During 2010 the modeled SST and observed SST are in very good agreement, both showing total anomalous warming of about 1.5°C between January and March (Fig. 12b). The model has more difficulty during 2015, especially in March, when observed SST cooled 1°C more than normal but the modeled SST shows slight anomalous warming (Fig. 12c). The discrepancy between model and observations during March 2015 will be discussed in more detail later in this section.

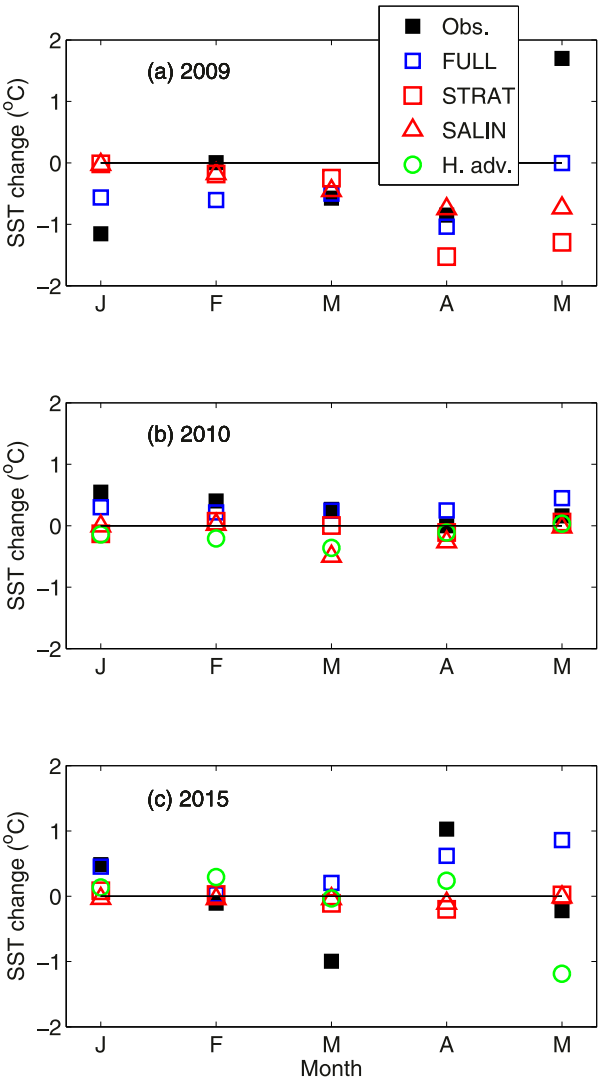

FIG. 12. Monthly change in SST at 4°N, 23°W from the one-dimensional mixed layer model experiments during January–May (a) 2009, (b) 2010, and (c) 2015. Filled black squares show observed changes; open blue squares are changes from the model with full forcing and initialization; red squares are with climatological surface momentum, heat, and freshwater fluxes; red triangles indicate climatological surface forcing and initialized each month with climatological ocean temperature. Green circles during 2010 and 2015 show the anomalous change in SST caused by horizontal temperature advection. Changes in SST for each month are calculated as the 5-day mean centered on the last day of the month minus the 5-day mean centered on the first day.

The disagreements between the model and observations in May 2009 and May 2015 may be caused by anomalous horizontal temperature advection, which is not included in the model and is difficult to quantify from observations. Foltz et al. (2012) showed anomalous warming of about 0.5°C from horizontal advection at 4°N, 23°W during May 2009, although with error bars as large as the signal. It is also possible that tropical instability waves may have caused strong temperature advection that is unrelated to the larger-scale SST patterns. Unfortunately, currents are not available from the mooring during the first half of 2009 to test these hypotheses. The other large discrepancy between the modeled and observed SST is in May 2015, when the model predicts approximately 1°C more warming compared to observations. In this case we have direct measurements of velocity from the mooring, which show that the warming is balanced by anomalous cooling from horizontal advection (Fig. 12c) associated with the passage of a tropical instability wave. In comparison, horizontal advection is much weaker during January–May 2010 (Fig. 12b) and January–April 2015.

2) PROCESSES RESPONSIBLE FOR THE 2009, 2010, AND 2015 EVENTS

The model experiment with climatological surface heat flux and wind stress forcing (STRAT experiment) shows no anomalous cooling during January 2009, consistent with observational results indicating that most of the cooling was caused by the surface heat flux (Fig. 12a). During March–May there is significant anomalous cooling even with climatological surface forcing, indicating that changes in ocean stratification and related changes in vertical turbulent cooling were very important. The model predicts anomalous cooling of about 2°C from vertical mixing during March–May 2009, consistent with observational results showing 2.3°C of anomalous cooling from vertical mixing in the region 2°–12°N, 15°–45°W, and about 1°–2°C of anomalous cooling at 4°N, 23°W during the same period (Foltz et al. 2012). The model results indicate that most of the anomalous cooling during March and April 2009 can be explained in terms of an anomalous shoaling of the thermocline and resultant enhancement of vertical turbulent cooling. Vertical mixing was also important in May 2009, acting to prolong the negative SST anomalies as the surface heat flux tended to damp them.

During April and May 2009 anomalous salinity stratification contributed significantly to the anomalous cooling from vertical mixing, based on the results of the experiment forced with climatological surface forcing and initialized with climatological temperature stratification (SALIN experiment; Fig. 12a). These months correspond to a period with lower than normal rainfall and higher than normal near-surface salinity at the mooring location, which would tend to decrease stratification and enhance turbulent mixing. Overall, it appears that most of the anomalous cooling during March–April 2009 can be explained by gradual anomalous shoaling of the thermocline and increasing surface salinity (on time scales of about a month or more). These changes acted to enhance vertical turbulent cooling. In contrast, the initial anomalous cooling in January was caused by changes in the surface heat flux.

During the positive AMM event in 2010, anomalous SST warming peaked in January and decreased gradually to zero by April (Fig. 12b). Most of the anomalous warming was driven by the surface heat flux (based on the good agreement between the observed monthly SST changes and those from the FULL experiment), in contrast to the strong contribution from stratification-induced changes in vertical mixing during 2009. There is also a strong contrast between the temporal evolution of SST anomalies during 2009 and 2010, which may be related to differences in meridional wind stress and upper-ocean thermal structure (Figs. 13a–f). During 2009 there is initial anomalous cooling of about 1°C between January and April, followed by abrupt anomalous cooling of about 1.5°C during early–mid April (Fig. 13a). In 2010, anomalous warming occurs more steadily during January–April, peaking at about 1.5°C in April (Fig. 13d). In both years, there were pronounced anomalies in meridional wind stress and thermocline depth. However, averaged during March–May the magnitudes of the anomalies were much larger during 2009. The meridional wind stress anomaly was $-0.021\,\mathrm{N\,m^{-2}}$ in 2009, compared to $0.009\,\mathrm{N\,m^{-2}}$ in 2010 (Figs. 13b,e). Consistent with the importance of meridional winds for generating Ekman pumping (Figs. 8 and 11g), the March–May thermocline depth anomaly in 2009 was −23 m compared to 12 m for the same period in 2010 (Figs. 13c,f). It is therefore possible that the weaker meridional wind stress and thermocline depth anomalies in 2010 caused vertical mixing to play a much smaller role in comparison to 2009, in turn leading to a steadier and weaker surface flux–induced change in SST in 2010.

In 2015 there was a short-lived negative AMM event that peaked in early April (Figs. 11a and 13g). The model reproduced the surface flux–induced damping of the cold anomaly during April, but failed to produce the observed anomalous cooling in March (Fig. 12c). The cooling cannot be explained by anomalous horizontal temperature advection, since the strongest negative SST anomalies during February–March 2015 were located northeast of the mooring location and surface currents were northeastward at the mooring. Instead, the anomalous cooling was likely driven by anomalous Ekman pumping

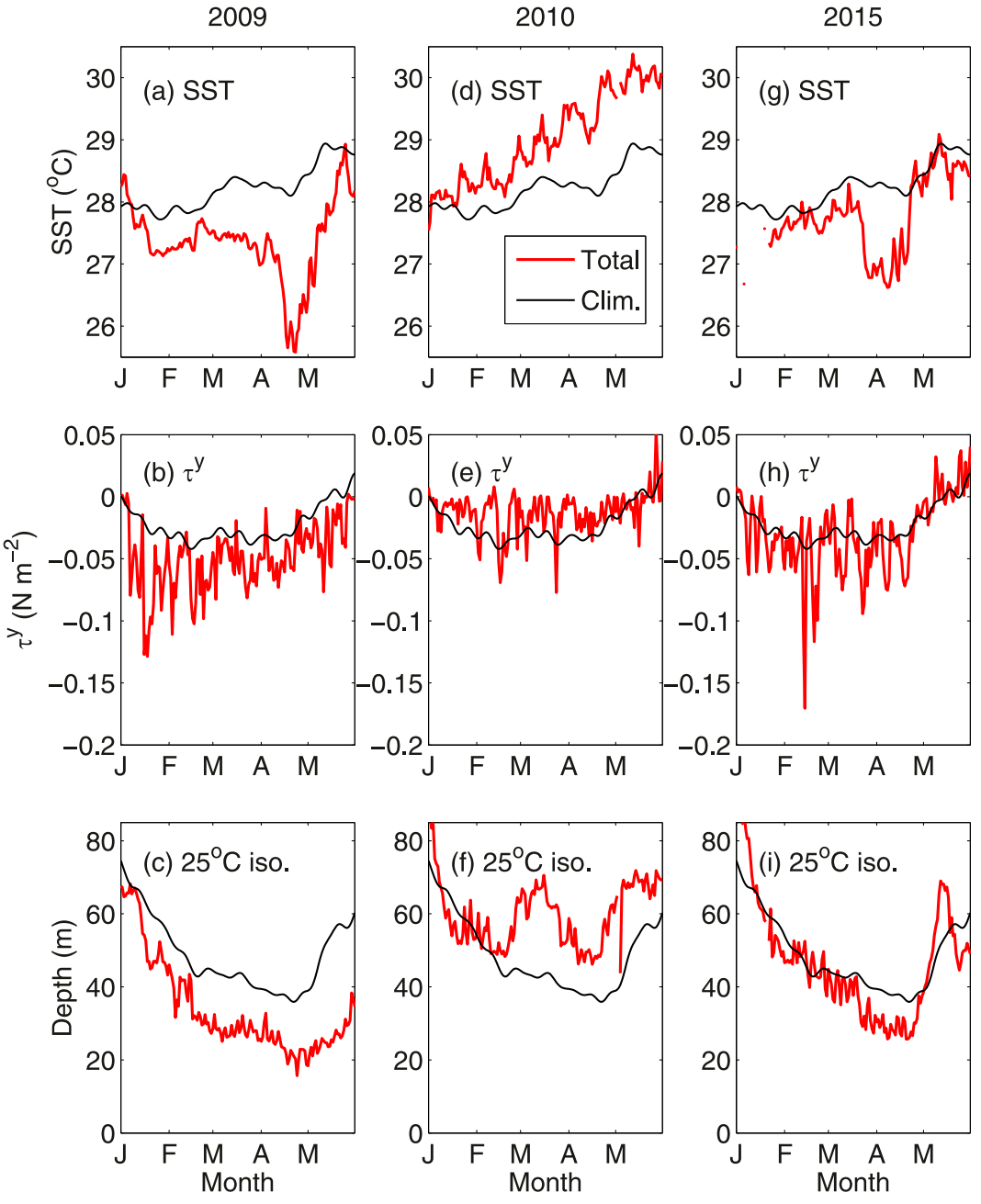

FIG. 13. Daily (red) and climatological (black) (a) SST, (b) meridional surface wind, and (c) depth of the 25°C isotherm from the PIRATA mooring at 4°N, 23°W during January–May 2009. (d)–(f) As in (a)–(c), but during 2010. (g)–(i) As in (a)–(c), but during 2015.

that occurred during the second half of March. Measurements from the mooring show a very abrupt anomalous decrease in SST during the end of March 2015 (Fig. 13g) that coincided with a sudden intensification of northerly (southward) wind stress from 0 to 0.1 N m^{-2} (Fig. 13h) and an abrupt anomalous shoaling of the thermocline (Fig. 13i). Anomalously strong southward winds were present in April, then switched to anomalously northward in May. The termination of the anomalously strong southward winds occurred as SST and thermocline depth rapidly returned to normal. The anomalous shoaling of the thermocline took place as its climatological depth reached a minimum of 40 m (Fig. 13i), likely allowing anomalous shoaling to significantly increase the vertical temperature gradient below the mixed layer and increase the rate of turbulent cooling of SST. These abrupt changes

are not well resolved in the monthly time series at the mooring location (Fig. 11) and not reproduced by the model (Fig. 12). However, there are striking similarities between the abrupt anomalous cooling of about 1°C in late March 2015 and about 1.5°C in early–mid April 2009: both occurred during periods of anomalous northerly wind stress, shallower than normal thermocline, and minimum seasonal mean thermocline depth. These similarities, combined with the one-dimensional modeling results, point to an important role for vertical mixing during these events.

Generally consistent with the mooring analysis (Figs. 9 and 11d), the modeled mixed layer deepened anomalously by 21 m between January and March 2009, shoaled 30 m during the same period in 2010, and shoaled 1 m in 2015. In addition to the important role of meridional wind-induced changes in thermocline depth, the composite analysis, mooring measurements, and model results therefore all indicate that there are anomalous changes in mixed layer depth in the TNA during AMM events. The timing of such events relative to climatological variations also seems to be important, with anomalous Ekman pumping altering SST most efficiently during March–May, when the thermocline is shallowest climatologically. The strong contribution from vertical mixing in April–May 2009, in contrast with much weaker vertical mixing–induced SST anomalies in April–May 2010, is consistent with the lack of a statistically significant residual in the composite analysis (Fig. 7b), which points to an inconsistent role for vertical mixing in the mixed layer temperature budget. The ultimate cause of year-to-year differences in vertical mixing is unclear and remains an important topic for future research. Some possibilities are discussed in the next section.

5. Summary and discussion

In this study we used composite analysis for 1982–2014 to investigate the upper-ocean response to the AMM and the processes that drive SST anomalies. We found that wind speed anomalies in the tropical Atlantic drive latent heat flux and mixed layer depth anomalies during boreal winter and spring, both of which contribute to the development of SST anomalies in the tropical North Atlantic associated with the AMM. Mixed layer depth anomalies are largest in the northern tropical Atlantic (15°–20°N) during boreal winter and shift southwestward during boreal spring. They affect the sensitivity of SST to the surface heat flux and contribute most strongly to SST anomalies (~0.5°–1°C month^{-1}) in the ITCZ region (2°–8°N) and western equatorial Atlantic, where the mixed layer depth anomalies are significant and the mean mixed layer is thin. Once the surface flux–induced SST anomalies develop, they are damped by SST-induced anomalies in latent heat flux in the eastern tropical North Atlantic and additionally by anomalies of surface shortwave radiation between 5°S and 10°N, where anomalies in ITCZ cloudiness and rainfall are most pronounced. During boreal spring we found significant thermocline depth anomalies in the ITCZ region, western tropical South Atlantic, and eastern equatorial Atlantic that are likely driven locally by Ekman pumping and remotely by equatorial Kelvin and Rossby waves. Despite significant thermocline depth anomalies and a shallow mean thermocline (<80 m) in the eastern ITCZ region, we found no evidence of a significant role for anomalous vertical turbulent cooling during a composite AMM. Results from a correlation analysis using direct measurements from 12 PIRATA moorings in the tropical North Atlantic during 1998–2014 are similar to the longer-period composite analysis.

Direct measurements from a mooring at 4°N, 23°W, located in a region with significant thermocline depth anomalies during AMM events, were used together with one-dimensional mixed layer model experiments to investigate further the impact of thermocline depth anomalies on SST in the ITCZ region. Three events were analyzed: two anomalous SST cooling episodes (2009 and 2015) that were associated with negative phases of the AMM, and an anomalous warming event (2010) associated with a positive phase of the AMM. We found significant event-to-event differences in the factors affecting SST at the mooring location. Results confirm the important role of vertical turbulent cooling during the development of the strong negative AMM event during March–May 2009 (Foltz et al. 2012) and the weaker and shorter-lived event in March–April 2015, but do not show a significant contribution from the vertical heat flux during the weaker positive AMM event in 2010. Anomalous turbulent cooling in 2009 and 2015 can be traced to anomalous northerly wind stress associated with a southward displacement of the ITCZ. These northerly wind stress anomalies, acting on the meridional gradient of planetary vorticity, generated anomalous upwelling and associated shoaling of the thermocline, allowing vertical turbulent mixing to cool SST more efficiently. Anomalous westerly winds on the equator also likely generated upwelling equatorial Rossby waves that may have enhanced the thermocline depth anomalies at 4°N. In contrast, during the 2010 warm event, March–May meridional wind stress and thermocline depth anomalies were considerably weaker than during the same period in 2009, resulting in a much smaller contribution from anomalies in vertical turbulent cooling. These pronounced differences during March–May were present despite similar magnitudes of the initial anomalous cooling and warming during January–February 2009 and 2010, respectively.

The reasons for the differences in the magnitudes and durations of the wind stress and thermocline depth anomalies during the 2009, 2010, and 2015 events are unclear, but may be related to preexisting SST anomalies along the equator in the central tropical Atlantic. Averaged between 15° and 30°W and during January–February, equatorial SST anomalies were 0.17°, 0.10°, and −0.25°C in 2009, 2010, and 2015, respectively. The positive equatorial SST anomalies during the 2009 cold event tended to increase the magnitude of the anomalous meridional SST gradient in the ITCZ region. This in turn may have led to stronger positive wind–evaporation–SST (WES), and possibly wind–upwelling–SST, feedback in the ITCZ region (2°–10°N), acting to intensify and prolong the wind stress, thermocline depth, and SST anomalies at 4°N. In contrast, during the 2010 and 2015 events, the preexisting equatorial SST anomalies tended to reduce the strength of the anomalous meridional SST gradient and these positive feedbacks, leading to a weaker event in 2010 and a shorter-duration event in 2015. Further investigation of these differences is warranted, given that the strong event in 2009 led to severe flooding in northeastern Brazil, whereas during 2010 and 2015 rainfall was close to normal. It is also possible that there is an asymmetry in the impact of thermocline depth anomalies on SST, with SST more sensitive to an anomalously shallower thermocline, although we did not find a significant asymmetry in the SST budget residual. Experiments with coupled models will be helpful for assessing the importance of initial SST conditions, upwelling asymmetry, positive WES feedback, and potentially wind–upwelling–SST feedback, during the development of AMM events.

Acknowledgments. This study was supported by a grant from the Climate Monitoring Program of NOAA's Climate Program Office. The research was carried out in part under the auspices of the Cooperative Institute for Marine and Atmospheric Studies (CIMAS), a Cooperative Institute of the University of Miami and NOAA, cooperative agreement NA10OAR4320143. Additional support was provided by NOAA's Atlantic Oceanographic and Meteorological Laboratory, and NOAA's Ernest F. Hollings Scholarship program. The authors thank the PIRATA program for making mooring and shipboard datasets freely available, and Paul Freitag, Michael McPhaden, Daniel Dougherty, Linda Stratton, and Michael Strick for answering questions and making the T-Flex temperature and salinity data available for our analysis. The authors thank Sang-Ki Lee and three anonymous reviewers, who provided insightful comments and suggestions that improved the manuscript, and Rick Lumpkin, who provided an updated version of the near-surface drifter-altimetry synthesis currents.

REFERENCES

Balmaseda, M. A., K. Mogensen, and A. T. Weaver, 2013: Evaluation of the ECMWF Ocean Reanalysis System ORAS4. *Quart. J. Roy. Meteor. Soc.*, **139**, 1132–1161, doi:10.1002/qj.2063.

Behringer, D. W., and Y. Xue, 2004: Evaluation of the global ocean data assimilation system at NCEP: The Pacific Ocean. *Eighth Symp. on Integrated Observing and Assimilation Systems for Atmosphere, Oceans, and Land Surface*, Seattle, WA, Amer. Meteor. Soc., 2.3. [Available online at https://ams.confex.com/ams/pdfpapers/70720.pdf.]

Bourlès, B., and Coauthors, 2008: The PIRATA program: History, accomplishments, and future directions. *Bull. Amer. Meteor. Soc.*, **89**, 1111–1125, doi:10.1175/2008BAMS2462.1.

Carton, J. A., and B. Huang, 1994: Warm events in the tropical Atlantic. *J. Phys. Oceanogr.*, **24**, 888–903, doi:10.1175/1520-0485(1994)024<0888:WEITTA>2.0.CO;2.

——, and B. S. Giese, 2008: A reanalysis of ocean climate using Simple Ocean Data Assimilation (SODA). *Mon. Wea. Rev.*, **136**, 2999–3017, doi:10.1175/2007MWR1978.1.

——, X. H. Cao, B. S. Giese, and A. M. da Silva, 1996: Decadal and interannual SST variability in the tropical Atlantic Ocean. *J. Phys. Oceanogr.*, **26**, 1165–1175, doi:10.1175/1520-0485(1996)026<1165:DAISVI>2.0.CO;2.

Chang, P., L. Ji, and H. Li, 1997: A decadal climate variation in the tropical Atlantic Ocean from thermodynamic air–sea interactions. *Nature*, **385**, 516–518, doi:10.1038/385516a0.

——, R. Saravanan, L. Ji, and G. C. Hegerl, 2000: The effect of local sea surface temperatures on atmospheric circulation over the tropical Atlantic sector. *J. Climate*, **13**, 2195–2216, doi:10.1175/1520-0442(2000)013<2195:TEOLSS>2.0.CO;2.

——, L. Ji, and R. Saravanan, 2001: A hybrid coupled model study of tropical Atlantic variability. *J. Climate*, **14**, 361–390, doi:10.1175/1520-0442(2001)013<0361:AHCMSO>2.0.CO;2.

Chiang, J. C. H., and D. J. Vimont, 2004: Analogous Pacific and Atlantic meridional modes of tropical atmosphere–ocean variability. *J. Climate*, **17**, 4143–4158, doi:10.1175/JCLI4953.1.

——, Y. Kushnir, and A. Giannini, 2002: Deconstructing Atlantic intertropical convergence zone variability: Influence of the local cross-equatorial sea surface temperature gradient and remote forcing from the eastern equatorial Pacific. *J. Geophys. Res.*, **107**, 4004, doi:10.1029/2000JD000307.

Czaja, A., P. Van der Vaart, and J. Marshall, 2002: A diagnostic study of the role of remote forcing in the tropical Atlantic variability. *J. Climate*, **15**, 3280–3290, doi:10.1175/1520-0442(2002)015<3280:ADSOTR>2.0.CO;2.

Dee, D. P., and Coauthors, 2011: The ERA-Interim reanalysis: Configuration and performance of the data assimilation system. *Quart. J. Roy. Meteor. Soc.*, **137**, 553–597, doi:10.1002/qj.828.

Doi, T., T. Tozuka, and T. Yamagata, 2010: The Atlantic meridional mode and its coupled variability with the Guinea Dome. *J. Climate*, **23**, 455–475, doi:10.1175/2009JCLI3198.1.

Enfield, D. B., and D. A. Mayer, 1997: Tropical Atlantic sea surface temperature variability and its relation to El Niño–Southern Oscillation. *J. Geophys. Res.*, **102**, 929–945, doi:10.1029/96JC03296.

Evan, A. T., G. R. Foltz, D. Zhang, and D. J. Vimont, 2011: Influence of African dust on ocean–atmosphere variability in the tropical Atlantic. *Nat. Geosci.*, **4**, 762–765, doi:10.1038/ngeo1276.

Fairall, C. W., E. F. Bradley, J. E. Hare, A. A. Grachev, and J. B. Edson, 2003: Bulk parameterization of air–sea fluxes: Updates and verification for the COARE algorithm. *J. Climate*, **16**, 571–591, doi:10.1175/1520-0442(2003)016<0571:BPOASF>2.0.CO;2.

Foltz, G. R., and M. J. McPhaden, 2006: The role of oceanic heat advection in the evolution of tropical North and South Atlantic SST anomalies. *J. Climate*, **19**, 6122–6138, doi:10.1175/JCLI3961.1.

——, and ——, 2010: Interaction between the Atlantic meridional and Niño modes. *Geophys. Res. Lett.*, **37**, L18604, doi:10.1029/2010GL044001.

——, ——, and R. Lumpkin, 2012: A strong Atlantic meridional mode event in 2009: The role of mixed layer dynamics. *J. Climate*, **25**, 363–380, doi:10.1175/JCLI-D-11-00150.1.

——, A. T. Evan, H. P. Freitag, S. Brown, and M. J. McPhaden, 2013a: Dust accumulation biases in PIRATA shortwave radiation records. *J. Atmos. Oceanic Technol.*, **30**, 1414–1432, doi:10.1175/JTECH-D-12-00169.1.

——, C. Schmid, and R. Lumpkin, 2013b: Seasonal cycle of the mixed layer heat budget in the northeastern tropical Atlantic Ocean. *J. Climate*, **26**, 8169–8188, doi:10.1175/JCLI-D-13-00037.1.

Graham, N. E., and T. P. Barnett, 1987: Sea surface temperature, surface wind divergence, and convection over tropical oceans. *Science*, **238**, 657–659, doi:10.1126/science.238.4827.657.

Ham, Y.-G., J.-S. Kug, J.-Y. Park, and F.-F. Jin, 2013: Sea surface temperature in the north tropical Atlantic as a trigger for El Niño/Southern Oscillation events. *Nat. Geosci.*, **6**, 112–116, doi:10.1038/ngeo1686.

Hu, Z.-Z., and B. Huang, 2006: Physical processes associated with tropical Atlantic SST meridional gradient. *J. Climate*, **19**, 5500–5518, doi:10.1175/JCLI3923.1.

Hummels, R., M. Dengler, P. Brandt, and M. Schlundt, 2014: Diapycnal heat flux and mixed layer heat budget within the Atlantic cold tongue. *Climate Dyn.*, **43**, 3179–3199, doi:10.1007/s00382-014-2339-6.

Keenlyside, N. S., and M. Latif, 2007: Understanding equatorial Atlantic interannual variability. *J. Climate*, **20**, 131–142, doi:10.1175/JCLI3992.1.

Kossin, J. P., and D. J. Vimont, 2007: A more general framework for understanding Atlantic hurricane variability and trends. *Bull. Amer. Meteor. Soc.*, **88**, 1767–1781, doi:10.1175/BAMS-88-11-1767.

Lumpkin, R., and S. Garzoli, 2011: Interannual to decadal changes in the western South Atlantic's surface circulation. *J. Geophys. Res.*, **116**, C01014, doi:10.1029/2010JC006285.

Mahajan, S., R. Saravanan, and P. Chang, 2010: Free and forced variability of the tropical Atlantic Ocean: Role of the wind–evaporation–sea surface temperature feedback. *J. Climate*, **23**, 5958–5977, doi:10.1175/2010JCLI3304.1.

Morel, A., and D. Antoine, 1994: Heating rate within the upper ocean in relation to its bio-optical state. *J. Phys. Oceanogr.*, **24**, 1652–1665, doi:10.1175/1520-0485(1994)024<1652:HRWTUO>2.0.CO;2.

Niiler, P. P., N. A. Maximenko, G. G. Panteleev, T. Yamagata, and D. B. Olson, 2003: Near-surface dynamical structure of the Kuroshio Extension. *J. Geophys. Res.*, **108**, 3193, doi:10.1029/2002JC001461.

Nobre, C., and J. Shukla, 1996: Variations of sea surface temperature, wind stress, and rainfall over the tropical Atlantic and South America. *J. Climate*, **9**, 2464–2479, doi:10.1175/1520-0442(1996)009<2464:VOSSTW>2.0.CO;2.

Perez, R. C., R. Lumpkin, W. E. Johns, G. R. Foltz, and V. Hormann, 2012: Interannual variations of Atlantic tropical instability waves. *J. Geophys. Res.*, **117**, C03011, 10.1029/2011JC007584.

Praveen Kumar, B. P., J. Vialard, M. Lengaigne, V. S. N. Murty, and M. J. McPhaden, 2012: TropFlux: Air–sea fluxes for the global tropical oceans—Description and evaluation. *Climate Dyn.*, **38**, 1521–1543, doi:10.1007/s00382-011-1115-0.

Price, J., R. Weller, and R. Pinkel, 1986: Diurnal cycling: Observations and models of the upper ocean response to diurnal heating, cooling, and wind mixing. *J. Geophys. Res.*, **91**, 8411–8427, doi:10.1029/JC091iC07p08411.

Reynolds, R. W., N. A. Rayner, T. M. Smith, D. C. Stokes, and W. Wang, 2002: An improved in situ and satellite SST analysis for climate. *J. Climate*, **15**, 1609–1625, doi:10.1175/1520-0442(2002)015<1609:AIISAS>2.0.CO;2.

Richter, I., S. K. Behera, Y. Masumoto, B. Taguchi, H. Sasaki, and T. Yamagata, 2013: Multiple causes of interannual sea surface temperature variability in the equatorial Atlantic Ocean. *Nat. Geosci.*, **6**, 43–47, doi:10.1038/ngeo1660.

Servain, J., 1991: Simple climatic indices for the tropical Atlantic Ocean and some applications. *J. Geophys. Res.*, **96**, 15 137–15 146, doi:10.1029/91JC01046.

Sweeney, C., and Coauthors, 2005: Impacts of shortwave penetration depth on large-scale ocean circulation and heat transport. *J. Phys. Oceanogr.*, **35**, 1103–1119, doi:10.1175/JPO2740.1.

Tanimoto, Y., and S. P. Xie, 2002: Interhemispheric decadal variations in SST, surface wind, heat flux, and cloud cover over the Atlantic Ocean. *J. Meteor. Soc. Japan*, **80**, 1199–1219, doi:10.2151/jmsj.80.1199.

Vimont, D. J., 2010: Transient growth of thermodynamically coupled variations in the tropics under an equatorially symmetric mean. *J. Climate*, **23**, 5771–5789, doi:10.1175/2010JCLI3532.1.

Wang, C., D. B. Enfield, S.-K. Lee, and C. W. Landsea, 2006: Influences of the Atlantic warm pool on Western Hemisphere summer rainfall and Atlantic hurricanes. *J. Climate*, **19**, 3011–3028, doi:10.1175/JCLI3770.1.

Xie, S.-P., 1999: A dynamic ocean–atmospheric model of the tropical Atlantic decadal variability. *J. Climate*, **12**, 64–70, doi:10.1175/1520-0442-12.1.64.

——, and J. A. Carton, 2004: Tropical Atlantic variability: Patterns, mechanisms, and impacts. *Earth's Climate: The Ocean–Atmosphere Interaction, Geophys. Monogr.*, Vol. 147, Amer. Geophys. Union, 121–142.

Yoon, J.-H., and N. Zeng, 2010: An Atlantic influence on Amazon rainfall. *Climate Dyn.*, **34**, 249–264, doi:10.1007/s00382-009-0551-6.

Yu, L. S., X. Z. Jin, and R. A. Weller, 2006: Role of net surface heat flux in seasonal variations of sea surface temperature in the tropical Atlantic Ocean. *J. Climate*, **19**, 6153–6169, doi:10.1175/JCLI3970.1.

Zhang, Y., W. B. Rossow, A. A. Lacis, V. Olnas, and M. I. Mishchenko, 2004: Calculation of radiative fluxes from the surface to top of atmosphere based on ISCCP and other global data sets: Refinements of the radiative transfer model and input data. *J. Geophys. Res.*, **109**, D19105, doi:10.1029/2003JD004457.